

Distance-driven binning for proton CT filtered backprojection along most likely paths

Simon Rit and Nicolas Freud and David Sarrut and Jean-Michel Létang

Abstract—We propose to account for curved most likely paths of protons in proton CT using an approximate adaptation of filtered backprojection algorithms. The protons are first binned in several proton radiographies at different distances to the source of protons. The adequate radiography is then used during backprojection depending on the distance to the source. The efficiency of the distance-driven binning on spatial resolution is demonstrated on a Monte Carlo simulated phantom with a circular trajectory and a cone-beam of protons.

I. INTRODUCTION

Proton computed tomography (pCT) has been considered very early in the history of CT [1] with a continuous development until the beginning of the eighties. This development was then slowed down because the ratio between benefits and cost was too low compared to photon CT scanners. In the nineties, the development of proton therapy has triggered new developments on pCT scanners [2].

There are indeed a few advantages of pCT over photon CT that are foreseen. The main expectation is the reduction of the uncertainty in the proton therapy planning due to the lack of accuracy of the proton stopping power computed from Hounsfield units [3]. Another potential benefit is the reduction of the imaging dose thanks to the Bragg curve characterizing the dose deposit of protons in matter [4], [5]. Finally, pCT is an additional modality which could have its own advantages for improving the diagnostic [6].

However, pCT has also one major drawback, its lack of spatial resolution. Indeed, protons traversing matter undergo multiple deflections due to Multiple Coulomb Scattering (MCS), resulting in curved trajectories and blurred proton radiographies [7]. Therefore, in the past decade, most efforts have focused on improving the spatial resolution of pCT by constructing most likely proton paths [5], [8], [9]. So far, these estimates have either been used to reconstruct pCT images using iterative algorithms [10], or to eliminate protons that had not followed straight lines before applying filtered back-projection (FBP) algorithms [4]. Indeed, to our knowledge, it is always claimed in pCT that FBP can only be applied to straight acquisition lines, probably because exact FBP has only been proposed along straight acquisition lines [11].

In this article, we propose a new FBP algorithm for pCT using curved most likely paths of protons. We have previously shown [12], as well as others, that approximate FBP

S. Rit, N. Freud, D. Sarrut and J.-M. Létang are with the Université de Lyon, CREATIS; CNRS UMR5220; Inserm U1044; INSA-Lyon; Université Lyon 1; Centre Léon Bérard, France (e-mail: simon.rit@creatis.insa-lyon.fr). This work is supported by the grant ProTom of the *ITMO Cancer et Technologie* in the *Plan Cancer 2009-2013* program.

algorithms for motion compensation along curved acquisition lines are efficient. The assumption of those algorithms is that local compensation of the deformation corrects for the motion blur and improves spatial resolution. In pCT, the problem is different because one records individual proton information which requires specific handling. We propose a distance-driven binning of protons in several radiographies located at different distances to the source to adapt the binning depending on the intersection of proton paths with each radiography.

II. PCT RECONSTRUCTION PROBLEM

Along its path, a proton loses most of its energy via inelastic collisions if it does not undergo nuclear interactions [13]. The local energy loss dE at point $\mathbf{x} \in \mathbb{R}^3$ is given by

$$-\frac{dE}{dx}(\mathbf{x}) = \eta(\mathbf{x})S(I(\mathbf{x}), E(\mathbf{x})) \quad (1)$$

where $\eta : \mathbb{R}^3 \rightarrow \mathbb{R}$ is the relative electron density with respect to a reference medium (water in this study), $S : \mathbb{R}^2 \rightarrow \mathbb{R}$ is the proton stopping power in water given by the Bethe-Bloch equation [14] and $I : \mathbb{R}^3 \rightarrow \mathbb{R}$ is the ionization potential which depends on the tissue characteristics.

The ionization potential I varies moderately in human tissues and has a limited effect on S so, in pCT, it is typically approximated to that of water, i.e., $I(\mathbf{x}) = I_{\text{water}} = 69 \text{ eV } \forall \mathbf{x} \in \mathbb{R}^3$ in our simulations. Under this assumption, integrating Equation 1 leads to the line integral

$$\int_{\Gamma_i} \eta(\mathbf{x}) d\mathbf{x} = \int_{E_i^{out}}^{E_i^{in}} \frac{1}{S(I_{\text{water}}, E)} dE = G(E_i^{in}, E_i^{out}) \quad (2)$$

with $\Gamma_i(t) \in \mathbb{R}^3$ the curved trajectory of the proton, function of time $t \in \mathbb{R}$, $i \in \mathbf{I} \subset \mathbb{Z}$ the proton index, E_i^{in} , E_i^{out} the entrance and exit energies of the proton, and $G : \mathbb{R}^2 \rightarrow \mathbb{R}$ the function that computes the energy integral from E_i^{in} and E_i^{out} , defined for simpler notations in the following. Finding η from E_i^{in} , E_i^{out} and an estimate of the path Γ_i for a set \mathbf{I} of protons is the pCT reconstruction problem.

Proton path estimation is a crucial problem in pCT reconstruction because it directly influences the spatial resolution [7]. Several solutions have been proposed to the problem of most likely path (MLP) estimation [5], [8], [9]. These recent works on MLP estimation rely on pCT scanners such as the apparatus described in [2] which measures the position and the direction of each proton, before and after traversing the object. Similarly, we assumed a cone-beam pCT scanner with a proton source following a circular trajectory $\mathbf{a}(t) \in \mathbb{R}^3$ around the axis defined by the isocenter $\mathbf{o} \in \mathbb{R}^3$ and the

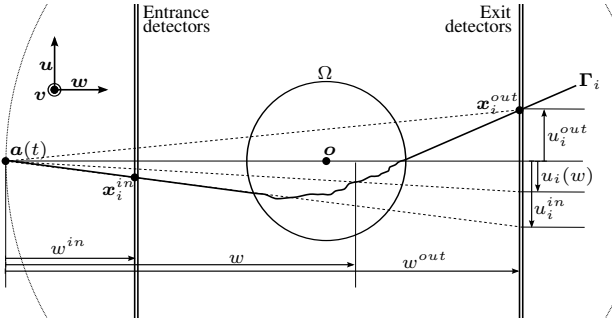


Fig. 1. Schematic top view of the pCT scanner used in this study. The signed distances w^{out} , w^{in} , w and u_i^{out} , u_i^{in} , $u_i(w)$ are used in Equation 4, 5 and 6, respectively.

unit axis $\mathbf{v} \in \mathbb{R}^3$, and two pairs of flat panels located before and after the scanned object to record their entrance and exit positions and directions $\mathbf{x}_i^{in}, \mathbf{x}_i^{out}, \dot{\mathbf{x}}_i^{in}, \dot{\mathbf{x}}_i^{out} \in \mathbb{R}^3$ (Figure 1). We define the unit vectors $\mathbf{u}, \mathbf{w} : \mathbb{R}^3 \rightarrow \mathbb{R}^3$ depending on the source position, with $\mathbf{w}(a(t)) = -\mathbf{a}(t)/\|\mathbf{a}(t)\|_2$ and $\mathbf{u}(a(t)) = \mathbf{v} \times \mathbf{w}(a(t))$, to have a 3D Cartesian coordinate system $\{\mathbf{u}, \mathbf{v}, \mathbf{w}\}$ rotating with the source and the detectors. We also assumed that the convex hull of the object $\Omega \subset \mathbb{R}^3$ was known which can practically be measured with a surface scanner or a rough initial reconstruction. The algorithm proposed in this work is applicable to any MLP estimation from measured spatial information ($\mathbf{x}_i^{in}, \dot{\mathbf{x}}_i^{in}, \mathbf{x}_i^{out}, \dot{\mathbf{x}}_i^{out}$ and Ω).

III. DISTANCE-DRIVEN BINNING

Our objective is to adapt existing filtered backprojection algorithms for pCT reconstruction. So far, previous works in that direction have binned proton information in virtual proton radiographies. Let $j \in \mathbf{J} \subset \mathbb{Z}^2$ be a set of spatial indices corresponding to a grid of pixels of the exit panel and $h : \mathbb{R}^2 \rightarrow \mathbb{R}$ their indicators,

$$h_j(\mathbf{y}) = \begin{cases} 1 & \text{if } \mathbf{y} \in \mathbb{R}^2 \text{ is in the } j^{\text{th}} \text{ pixel,} \\ 0 & \text{else.} \end{cases} \quad (3)$$

The virtual proton radiography binned at the exit detector for a subset of protons $\mathbf{I}_a \subset \mathbf{I}$ emitted from a same source position \mathbf{a} is

$$g_{j,a}^{out} = \frac{\sum_{i \in \mathbf{I}_a} h_j(u_i^{out}, v_i^{out}) G(E_i^{in}, E_i^{out})}{\sum_i h_j(u_i^{out}, v_i^{out})} \quad (4)$$

with $u_i^{out} = (\mathbf{x}_i^{out} - \mathbf{a}) \cdot \mathbf{u}(\mathbf{a})$ and $v_i^{out} = (\mathbf{x}_i^{out} - \mathbf{a}) \cdot \mathbf{v}$ (Figure 1). Repeating this operation for several source positions, one obtains a typical set of projection images g^{out} that can be used in a standard filtered-backprojection algorithm.

We observe that one could also use the entrance positions \mathbf{x}_i^{in} to bin projection images on the exit detector assuming a straight path going through \mathbf{x}_i^{in} and the source \mathbf{a} , i.e.

$$g_{j,a}^{in} = \frac{\sum_{i \in \mathbf{I}_a} h_j(u_i^{in}, v_i^{in}) G(E_i^{in}, E_i^{out})}{\sum_i h_j(u_i^{in}, v_i^{in})} \quad (5)$$

with the distances illustrated in Figure 1

$$\begin{cases} u_i^{in} = \frac{w^{out}}{w^{in}} ((\mathbf{x}_i^{in} - \mathbf{a}) \cdot \mathbf{u}(\mathbf{a})), & w^{in} = (\mathbf{x}_i^{in} - \mathbf{a}) \cdot \mathbf{w}(\mathbf{a}), \\ v_i^{in} = \frac{w^{out}}{w^{in}} ((\mathbf{x}_i^{in} - \mathbf{a}) \cdot \mathbf{v}), & w^{out} = (\mathbf{x}_i^{out} - \mathbf{a}) \cdot \mathbf{w}(\mathbf{a}). \end{cases}$$

The ratio $\frac{w^{out}}{w^{in}}$ is the constant magnification from the entrance to the exit detection plane produced by a cone-beam focused on \mathbf{a} to obtain the coordinates on the exit flat panel. Therefore, if protons were travelling along straight paths, g^{in} and g^{out} would be equal. They are actually different due to MCS.

From this observation, we introduce the concept of distance-driven binning given by

$$g_{j,a}(w) = \frac{\sum_{i \in \mathbf{I}_a} h_j(u_i(w), v_i(w)) G(E_i^{in}, E_i^{out})}{\sum_i h_j(u_i(w), v_i(w))} \quad (6)$$

with the distances illustrated in Figure 1

$$\begin{cases} u_i(w) = \frac{w^{out}}{w} ((\Gamma_i(t_{i,w}) - \mathbf{a}) \cdot \mathbf{u}(\mathbf{a})), \\ v_i(w) = \frac{w^{out}}{w} ((\Gamma_i(t_{i,w}) - \mathbf{a}) \cdot \mathbf{v}). \end{cases}$$

$t_{i,w}$ is the time at which proton i crosses the plane parallel to the detectors at distance w from the source, i.e., $(\Gamma_i(t_{i,w}) - \mathbf{a}) \cdot \mathbf{w}(\mathbf{a}) = w$. Equation 6 is the extension of Equation 4 and 5 to any distance w using the most likely path Γ_i of proton i to interpolate intermediate positions between entrance and exit positions \mathbf{x}_i^{in} and \mathbf{x}_i^{out} . Indeed, as the trajectory Γ_i crosses the detectors at positions \mathbf{x}_i^{in} and \mathbf{x}_i^{out} , we have $g(w^{out}) = g^{out}$ and $g(w^{in}) = g^{in}$.

In practice, g is computed at a finite number of distances in the \mathbf{w} direction and linear interpolation is used between voxels g_j . In combination with bilinear interpolation between spatial indices j , we obtain a 4D sinogram $g : \mathbb{R}^3 \times \mathbb{Z} \rightarrow \mathbb{R}$ instead of the conventional 3D sinogram, e.g. $g^{out} : \mathbb{R}^2 \times \mathbb{Z} \rightarrow \mathbb{R}$, where the last dimension is the index of projection images.

IV. DISTANCE-DRIVEN BACKPROJECTION

We use the distance-driven binning in a filtered backprojection algorithm adapted from the Feldkamp-Davis-Kress (FDK) algorithm [15]. As in approximate motion-compensated cone-beam CT [12], we do not modify the 2D processing of projections in the FDK algorithm (the 2D weighting and the ramp filtering) but we repeat it for every depth w . We call \tilde{g}_a this 3D filtered projection at position source \mathbf{a} corresponding to a source angle $\theta_a \in \mathbb{R}$. We use this filtered distance-driven sinogram by accounting during backprojection for the distance to the source of the voxel being backprojected to select the adequate part of the distance-binned sinogram, i.e.

$$\eta(\mathbf{x}) = \int_0^{2\pi} \left(\frac{\|\mathbf{a}\|_2}{w(\mathbf{x})} \right)^2 \tilde{g}_a(u(\mathbf{x}), v(\mathbf{x}), w(\mathbf{x})) d\theta_a \quad (7)$$

with $u(\mathbf{x}) = \frac{w^{out}}{w(\mathbf{x})} ((\mathbf{x} - \mathbf{a}) \cdot \mathbf{u})$, $v(\mathbf{x}) = \frac{w^{out}}{w(\mathbf{x})} ((\mathbf{x} - \mathbf{a}) \cdot \mathbf{v})$ and $w(\mathbf{x}) = (\mathbf{x} - \mathbf{a}) \cdot \mathbf{w}$. It is worth noting that both the backprojection and its FDK weighting are driven by the same distance to the source $w(\mathbf{x})$.

V. EXPERIMENTS

The algorithm was evaluated with Monte-Carlo simulations using the latest release of GATE [16], an end-user software using the Geant4 toolkit [17]. GATE was run on the EGEE computing grid with the GateLab applet [18]. An ideal pCT scanner was simulated: a 200 MeV mono-energetic point source was placed at distance $w^s = -100$ cm from the

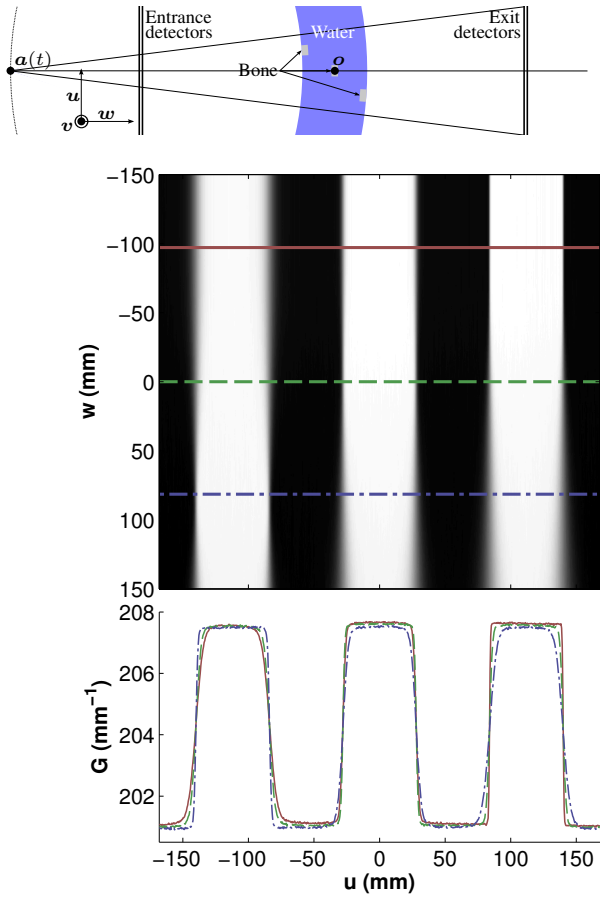


Fig. 2. Experiment 1. Top: drawing of the object. Middle: axial slice at the isocenter of the distance driven binning. Bottom: profiles along the three lines drawn on the top image.

isocenter and the characteristics (E_i^{in} , E_i^{out} , x_i^{in} , \dot{x}_i^{in} , x_i^{out} and \dot{x}_i^{out}) of protons traversing the planes $w^{in} = -60$ cm and $w^{out} = 60$ cm were recorded.

Standard 3σ cuts on energy and angle were applied to eliminate nuclear interactions [13]. Most likely paths Γ_i were estimated as straight paths outside Ω and curved paths in Ω according to the maximum likelihood formalism of Schulte *et al* [9]. The object was assumed to be homogeneous and made of water. We closely followed their work for its parameterization.

A. Experiment 1

The first experiment was designed to provide the reader with insights into the effect of the distance-driven binning by looking at one projection image only. We centered a spherical shell of water with radii 90 cm and 110 cm around the proton source, therefore placing the isocenter in the middle of the water layer (Figure 2, top). Three spherical bone inserts with identical solid angles were placed in the water sphere with regular radii from the source (90/92 cm, 99/101 cm and 108/110 cm). Since all objects are portions of hollow spheres centered on the source, the projection image for particles travelling along straight lines crossing the source would be a rectangular function with one rectangle per insert.

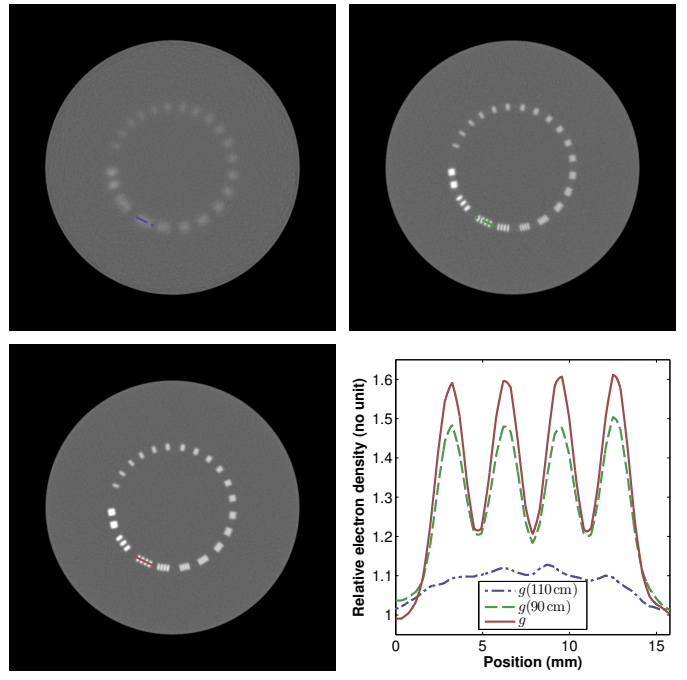


Fig. 3. Experiment 2, full scan. Top-left: axial slice at the isocenter of the standard FDK reconstruction using the 2D set of projection images $g(110 \text{ cm})$ binned according to the position of protons at the exit of the object. Gray window: [0.6, 1.6]. Top-right: idem with the sinogram $g(90 \text{ cm})$ at the entrance of the object. Bottom-left: distance-driven FDK reconstruction using the complete set of 3D projections g . Bottom-right: profile along the three segments drawn on each slice.

B. Experiment 2

The second experiment was designed to evaluate the spatial resolution of reconstructed pCT images (Figure 3). We used a resolution phantom similar to the CTP528 high-resolution module of the Catphan phantom (The Phantom Laboratory, Salem NY, USA): various resolution gauges made of 2 mm-thick aluminium sheets were placed on a circle ($\varnothing 10$ cm) in a water cylinder ($\varnothing 20$ cm).

VI. RESULTS

A. Experiment 1

Figure 2 is an illustration of the effect of distance-driven binning in the projection space. The effect of MCS depended on the distance to the source and the position of the inserts. The edges of the bone inserts were the sharpest at the distance which corresponds to their location in space, i.e. at the level of each line profile (Figure 2, bottom). The loss of sharpness increased with the distance to their location. We also observed that the middle insert was not as sharp on the central profile as the entrance and exit insert on their respective profile because the uncertainty on the estimate of the proton path was higher in the middle of the object than on the borders of the object.

B. Experiment 2

The effect on the reconstruction is shown in Figure 3. The spatial resolution improved with the distance binning compared to the spatial resolution of reconstruction using a

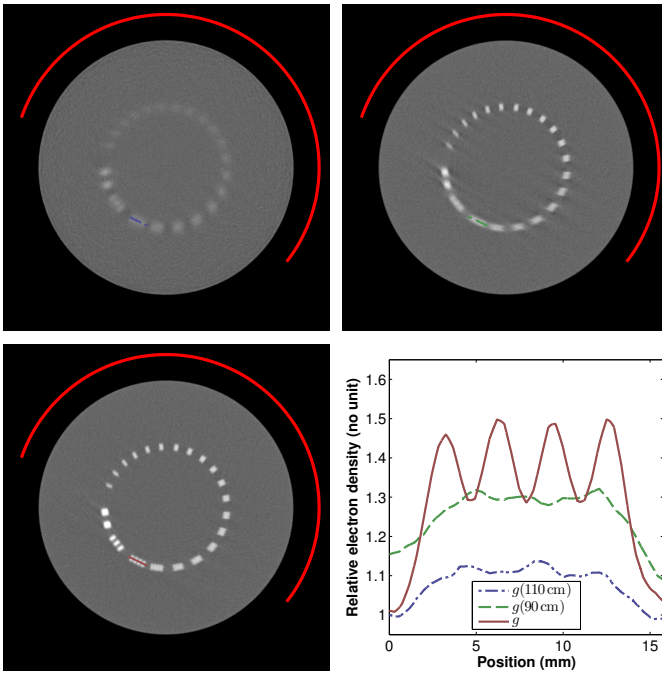


Fig. 4. Experiment 2, short scan. Idem as Figure 3 with an additional circle arc indicating the source trajectory at a false scale ($\varnothing 24\text{ cm}$ on the figure instead of $\varnothing 200\text{ cm}$).

standard set of binned projections (Figure 3, bottom left vs. top). We also observed that using the binning g^{in} according to the position of protons before the object is more efficient than using the binning g^{out} according to their exit position (Figure 3, top right vs. top left).

The effect is emphasized when only a subset of projection images is used which corresponds to a short scan (Figure 4). Parker weighting [19] was used to account for the short scan in the reconstructions of Figure 4.

VII. DISCUSSION AND CONCLUSION

We have proposed an algorithm to use curved most likely paths in a pCT filtered backprojection algorithm. Our solution uses a distance driven binning in order to recover sharp edges at the distance where the edge is located in space (Figure 2). During backprojection, the spatial position of each voxel is translated to a distance to the source and the corresponding position of the distance-driven binning is used so that, at the location of each edge, its sharpest binning is used.

This FBP algorithm is as approximate as other FBP algorithms used in pCT since there is no exact solution for curved trajectories. We observed an improved spatial resolution without apparent loss in density resolution (Figure 3) because the algorithm only modifies high frequencies of the sinogram without modifying low frequencies. The algorithm is inspired by our experience in approximate motion compensated FBP reconstruction where limited differences have been observed with iterative reconstruction [12]. However, comparison with existing pCT iterative algorithms will provide a better quantification of the effect of this approximation.

The major advantage of our algorithm over iterative pCT algorithms is faster and on-the-fly reconstruction. These assets

could become essential for their use in proton therapy treatment rooms when the reconstructed image is required to check the patient anatomy prior to starting the treatment. In this context, a short scan could also greatly reduce the acquisition time and the imaging dose, for which the use of most likely paths seems crucial.

REFERENCES

- [1] A.M. Cormack, "Representation of a function by its line integrals, with some radiological applications," *Journal of Applied Physics*, vol. 34, no. 9, pp. 2722–2727, 1963.
- [2] R. Schulte *et al.*, "Conceptual design of a proton computed tomography system for applications in proton radiation therapy," *IEEE Transactions on Nuclear Science*, vol. 51, no. 3, pp. 866–872, 2004.
- [3] B. Schaffner and E. Pedroni, "The precision of proton range calculations in proton radiotherapy treatment planning: experimental verification of the relation between CT-HU and proton stopping power," *Phys Med Biol*, vol. 43, no. 6, pp. 1579–1592, 1998.
- [4] G.A.P. Cirrone *et al.*, "Monte carlo evaluation of the filtered back projection method for image reconstruction in proton computed tomography," *Nucl Inst Meth A*, vol. 658, no. 1, pp. 78–83, 2011.
- [5] D. Wang, T.R. Mackie, and W.A. Tomé, "Bragg peak prediction from quantitative proton computed tomography using different path estimates," *Phys Med Biol*, vol. 56, no. 3, pp. 587–599, 2011.
- [6] N. Depauw and J. Seco, "Sensitivity study of proton radiography and comparison with kV and MV x-ray imaging using GEANT4 monte carlo simulations," *Phys Med Biol*, vol. 56, no. 8, pp. 2407–2421, 2011.
- [7] U. Schneider and E. Pedroni, "Multiple coulomb scattering and spatial resolution in proton radiography," *Med Phys*, vol. 21, no. 11, pp. 1657–1663, 1994.
- [8] D.C. Williams, "The most likely path of an energetic charged particle through a uniform medium," *Phys Med Biol*, vol. 49, no. 13, pp. 2899–2911, 2004.
- [9] R. W. Schulte, S. N. Penfold, J. T. Tafas, and K. E. Schubert, "A maximum likelihood proton path formalism for application in proton computed tomography," *Med Phys*, vol. 35, no. 11, pp. 4849–4856, 2008.
- [10] S. Penfold, "Image reconstruction and monte carlo simulations in the development of proton computed tomography for applications in proton radiation therapy," Ph.D. dissertation, University of Wollongong, 2010.
- [11] L. Desbat, S. Roux, and P. Grangeat, "Compensation of some time dependent deformations in tomography," *IEEE Trans Med Imaging*, vol. 26, no. 2, pp. 261–269, 2007.
- [12] S. Rit, D. Sarrut, and L. Desbat, "Comparison of analytic and algebraic methods for motion-compensated cone-beam CT reconstruction of the thorax," *IEEE Trans Med Imag*, vol. 28, no. 10, pp. 1513–1525, 2009.
- [13] R.W. Schulte, V. Bashkirov, M.C. Loss Klock, T. Li, A.J. Wroe, I. Evseev, D.C. Williams, and T. Satogata, "Density resolution of proton computed tomography," *Med Phys*, vol. 32, no. 4, pp. 1035–1046, 2005.
- [14] K Nakamura and Particle Data Group, "Review of particle physics," *Journal of Physics G: Nuclear and Particle Physics*, vol. 37, no. 7A, p. 075021, 2010.
- [15] L.A. Feldkamp, L.C. Davis, and J.W. Kress, "Practical cone-beam algorithm," *J Opt Soc Am A*, vol. 1, no. 6, pp. 612–619, 1984.
- [16] S. Jan *et al.*, "GATE V6: a major enhancement of the GATE simulation platform enabling modelling of CT and radiotherapy," *Phys Med Biol*, vol. 56, no. 4, pp. 881–901, 2011.
- [17] S. Agostinelli *et al.*, "Geant4-a simulation toolkit," *Nuclear Instruments and Methods in Physics Research Section A: Accelerators, Spectrometers, Detectors and Associated Equipment*, vol. 506, no. 3, pp. 250–303, 2003.
- [18] S. Camarasu-Pop, T. Glatard, J.T. Moscicki, H. Benoit-Cattin, and D. Sarrut, "Dynamic partitioning of GATE monte-carlo simulations on EGEE," *Journal of Grid Computing*, vol. 8, no. 2, pp. 241–259, 2010.
- [19] D.L. Parker, "Optimal short scan convolution reconstruction for fanbeam CT," *Med Phys*, vol. 9, no. 2, pp. 254–257, 1982.